water

MDPI

Article

Risk Assessment of Tunnel Water Inrush Based on Hybrid Optimisation Algorithms: A Case Study in Southwest China

Yue Huang [1], Peiru Li [2,*], Sixie Fu [3], Lingtao Zeng [1], Hanying Su [4] and Ruilang Cao [2]

[1] Guangxi Water & Power Design Institute Co., Ltd., Nanning 530015, China; haohan123qaz@gmail.com (Y.H.); hao965050137@foxmail.com (L.Z.)
[2] State Key Laboratory of Watershed Water Cycle and Water Security, China Institute of Water Resources and Hydropower Research, Beijing 100048, China; caorl@iwhr.com
[3] School of Intelligent Construction, Jilin University of Architecture and Technology, Changchun 130114, China; junw70712@gmail.com
[4] Guangxi Beibu Gulf Rim Water Diversion Co., Ltd., Nanning 530015, China; cotton@yeah.net
* Correspondence: p.r.li@email.cugb.edu.cn

Abstract

Tunnel water inrush risk assessment poses a complex multi-attribute decision-making challenge, garnering significant global attention as a critical yet unresolved issue in geotechnical engineering. While the Attribute Interval Recognition Theory (AIRT) has been widely adopted for geological hazard prediction, its application in tunnel water inrush scenarios often faces limitations in precise index attribute quantification and risk probability estimation. To address these constraints, this study proposes an improved integrated model combining AIRT, the Analytic Hierarchy Process (AHP), the Inverse Entropy Method (IEM), Game Theory (GT), the Technique for Order Preference by Similarity to Ideal Solution (TOPSIS), and Monte Carlo random simulation technology. In this framework, AHP and IEM are used to determine subjective and objective weights, GT is used to optimise the combined weights, TOPSIS is introduced to determine the index attribute measure coefficients, and Monte Carlo simulation is employed to estimate risk probabilities. The novelty of the model lies in improving both risk attribute identification and probabilistic assessment under interval-valued index conditions. The model was validated using 20 representative tunnel water inrush cases, demonstrating robust performance in capturing dynamic risk scenarios. When the confidence level was set to 0.65, all 20 cases were correctly classified, achieving an accuracy of 100%. Subsequently, the model was applied to the inlet section of the Nafeng Tunnel. The results show that the assessed section is classified as Class II, with risk probabilities of 0.515 and 1.000 for the D0 + 220.6–D0 + 285 m and D0 + 285–D0 + 340.6 m sections, respectively. These findings indicate that the proposed model can provide a quantitative basis for tunnel water inrush risk assessment and prevention.

Keywords: water inrush; evaluation model; risk probability; risk attribute identification; attribute measure

Check for updates

Academic Editor: Dan Ma

Received: 27 April 2026
Revised: 21 May 2026
Accepted: 27 May 2026
Published: 29 May 2026

Copyright: © 2026 by the authors. Licensee MDPI, Basel, Switzerland. This article is an open access article distributed under the terms and conditions of the Creative Commons Attribution (CC BY) license.

1. Introduction

With the deepening implementation of Water Transfer Projects in China, the amount of long water conveyance tunnels continues to increase. The geological conditions along the route are complex and varied, and geological hazards, such as face water inrush and mud inrush, are frequently exposed during tunnel construction, as illustrated in Figure 1. Among them, water inrush is one of the common types of geological hazards

in tunnel construction [1–3]. According to incomplete statistics, water inrush accounts for a substantial proportion of tunnel construction hazards in China [4]. Reported tunnel water inrush and mud inrush cases may involve different inrush materials and a wide range of water-inflow magnitudes. Figure 2 summarises the disaster-type distribution and water-inflow magnitude distribution based on previously reported cases [2,4–6]. In Figure 2a, the cases are classified according to the main disaster-causing type, namely fault-related, karst-related, and other types, and the left axis indicates the corresponding number of reported cases. Therefore, this panel is intended to show the distribution of reported water and mud inrush disasters by geological type, rather than to distinguish water-only inrush from mud-only inrush. Figure 2b further presents the distribution of water-inflow magnitude among these reported cases. For example, more than five water inrush accidents occurred in the Bieyancao tunnel, at least six water inrush accidents occurred in the Qiyue Mountain tunnel of Yiwan Railway, and several water inrush accidents occurred in the Dayao Mountain tunnel [6]. In addition, tunnel water inrush disasters occurred frequently in countries such as Japan and Norway [7–9]. The water inrush seriously threatens the normal construction of tunnels. Effective prevention of tunnel water inrush has become a global difficulty and hotspot that urgently needs to be solved.



(**a**) (**b**)

Figure 1. Field photographs of typical water and mud inrush phenomena. (**a**) Face water inrush at the Yunkaishan Tunnel, (**b**) mud inrush at the Jiling Tunnel.

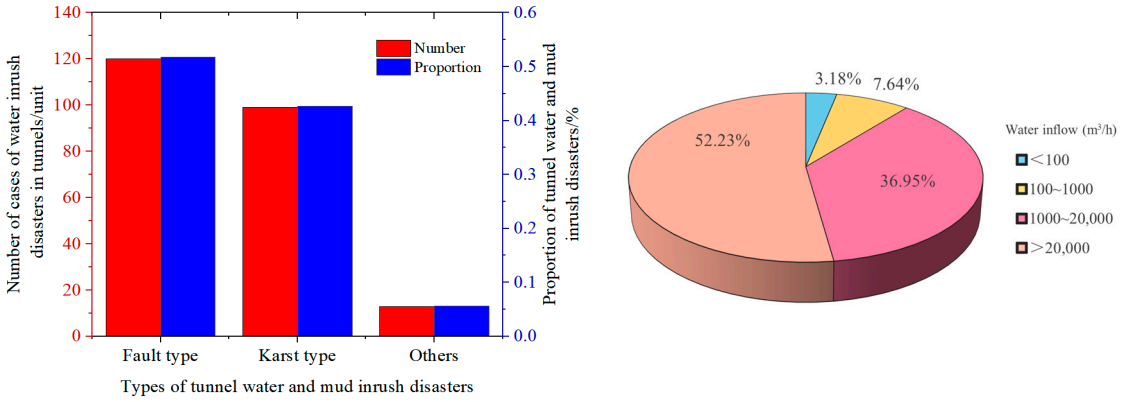

(**a**) (**b**)

Figure 2. Characteristics of tunnel water inrush disasters [2,4–6]. (**a**) Distribution of reported cases by main disaster-causing type, (**b**) distribution of water-inflow magnitude.

Risk assessment plays an important role in understanding the behaviour of water inrush, which is an important foundation for risk control of tunnel water inrush disasters. The common methods include on-site monitoring [10,11], physical model experiments [12–19], numerical simulation [20–25], machine learning [26–28], and multi-attribute decision-making methods [5,29–31]. Neural-network-based approaches have also been applied to sensitivity analysis of key parameters in rock engineering problems, such as borehole failure, demonstrating their potential for identifying influential factors in geotechnical risk assessment [32]. The multi-attribute decision-making method performs outstandingly in dealing with the uncertainty and ambiguity of the object, and has the advantages of low cost, strong ability to process multi-source information fusion, and good adaptability to indicator data types, which has been widely used in the early prediction of tunnel water inrush disasters. Li et al. [5] proposed an improved evidence theory for the risk assessment of tunnel water inrush based on the precursor information of water inrush measured by physical model experiments. Wang et al. [33] proposed a method for predicting and warning of water inrush in tunnels by integrating evidence theory and advanced geological forecasting techniques. Zhang et al. [34] proposed a risk assessment method for tunnel water inrush based on quantitative analysis of multi-objective optimisation and proximity model and verified it in a tunnel in southern China. Kong et al. [35] proposed a tunnel water inrush disaster risk assessment model to address the uncertainty and ambiguity of tunnel water inrush disasters. This method used the Fuzzy Analytic Hierarchy Process (FAHP) to determine the weights of each evaluation index and the improved ideal solution theory (I-TOPSIS) to evaluate the risk level.

The risk assessment of tunnel water inrush based on multi-attribute decision-making theory relies on the effective identification of indices. However, lots of engineering practices have shown that there is a certain degree of uncertainty in the quantitative characterisation of indices, often manifested as interval values. Different values of the index may lead to the possibility of multiple attributes, which is one of the reasons for the ambiguity of the evaluation results. Therefore, it is more reasonable to use interval value representation for indices. The AIRT is an extension of attribute recognition theory, which quantitatively characterises indices using the attribute measure [36]. The index attribute measure is dimensionless and can effectively reduce the impact of different units of indices. Secondly, the AIRT uses interval values to characterise the indices, and it can better reflect the uncertainty impact of the index. Furthermore, it adopts confidence criteria, which can effectively solve the problem of multiple peaks compared with the maximum membership principle, to identify the risk levels [36–39].

However, the AIRT method still has certain limitations in dealing with the index attribute measure and risk probability. The testing results are usually interval values, and the comprehensive index attribute measure was often calculated using the equalisation coefficient method [40,41], with a value of 0.5. The existing achievements had not taken into account the influence of preference within the attribute measure interval of the testing results. In addition, the risk probability is an important consideration for the risk of tunnel water inrush. Zhou et al. [40] determined the risk probability based on the combination of upper and lower limits of the measure interval. However, this method ignored the influence of the median value. There is a certain deviation between the evaluation results of tunnel water inrush and the actual situation.

Although AIRT provides a suitable framework for describing interval-valued indices and identifying fuzzy risk attributes, its conventional application still has limitations in determining attribute measure coefficients and estimating risk probability. Therefore, this study integrates AHP, IEM, GT, TOPSIS, and Monte Carlo simulation with AIRT to improve the weighting of risk indices, the calculation of comprehensive attribute measures, and

the estimation of risk probability. To clarify the methodological basis of the proposed hybrid model, the strengths, limitations, and roles of the methods used in this study are summarised in Table 1.

Table 1. Summary of the methods used in the proposed hybrid risk assessment model.

Method	Strengths	Limitations	Role in This Study
AIRT	Handles interval-valued indices and fuzzy risk attributes	Attribute measure calculation and risk probability estimation need improvement	Provides the basic framework for risk attribute identification
AHP	Reflects expert judgement and engineering experience	Depends on subjective judgement	Determines subjective weights of risk indices
IEM	Provides objective weights based on measured data	Affected by the reliability of measured data	Determines objective weights of risk indices
GT	Coordinates subjective and objective weighting results	Depends on the initial weighting results	Combines AHP and IEM weights
TOPSIS	Calculates closeness to ideal solutions	Depends on the defined ideal points	Determines the attribute measure coefficient
Monte Carlo simulation	Simulates possible values within measured intervals	Requires predefined index intervals	Estimates the probability of each risk level

To overcome the above shortcomings, the present study integrates AHP, IEM, GT, TOPSIS, and Monte Carlo simulation into the AIRT framework. AHP and IEM are used to determine subjective and objective weights, GT is adopted to obtain combined weights, TOPSIS is introduced to improve the calculation of attribute measure coefficients, and Monte Carlo simulation is used to estimate risk probability. Accordingly, an improved risk attribute interval identification model for tunnel water inrush is established to better reflect its fuzzy and uncertain characteristics and to improve the efficiency and accuracy of risk prediction. The results are expected to provide a useful reference for the risk assessment and prevention of tunnel water inrush disasters in China.

2. Methodology

2.1. Hybrid Optimisation Framework

The tunnel water inrush is the result of the coupling effect of internal factors, such as hydrogeological and engineering geological conditions, and external factors, such as excavation disturbance. To ensure the rationality of the selected evaluation indices, the factors were determined based on the dominant mechanisms of tunnel water inrush and expert consultation. Specifically, tunnel water inrush is mainly controlled by water source conditions, water-conducting structures, geological barriers, and external recharge. Formation lithology and rock quality reflect the water-resisting capacity of the surrounding rock; groundwater level represents the hydraulic driving force; topography and rainfall characterise groundwater recharge conditions; and strata attitude and unfavourable geological conditions describe the structural conditions and potential water-conducting pathways.

Specifically, 28 senior experts in relevant fields were consulted to evaluate the importance of the disaster-causing factors of tunnel water inrush, including five technical personnel from design institutes, seven researchers from scientific research institutes, eight professors from universities, four technical personnel from construction companies, and four management personnel from construction units. Seven categories of factors were selected, including formation lithology, groundwater level, topography, strata attitude, rock

quality, unfavourable geological conditions, and rainfall. To make these categories applicable to the proposed evaluation model, they were further represented by nine evaluation indices: formation lithology, groundwater level, negative topography area ratio, annual average rainfall, corrected strata angle, rock quality, fold distribution, fault properties, and fault width. Among them, the category of unfavourable geological conditions was represented by three specific indices, namely fold distribution, fault properties, and fault width. The expert-evaluation results are shown in Figure 3, and the risk assessment index system for tunnel water inrush is shown in Figure 4.

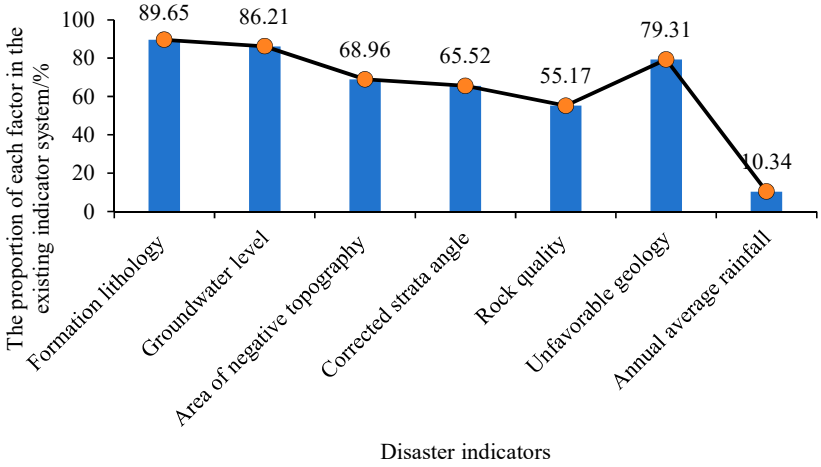

Figure 3. Evaluation of disaster-causing factors of water inrush in tunnels.

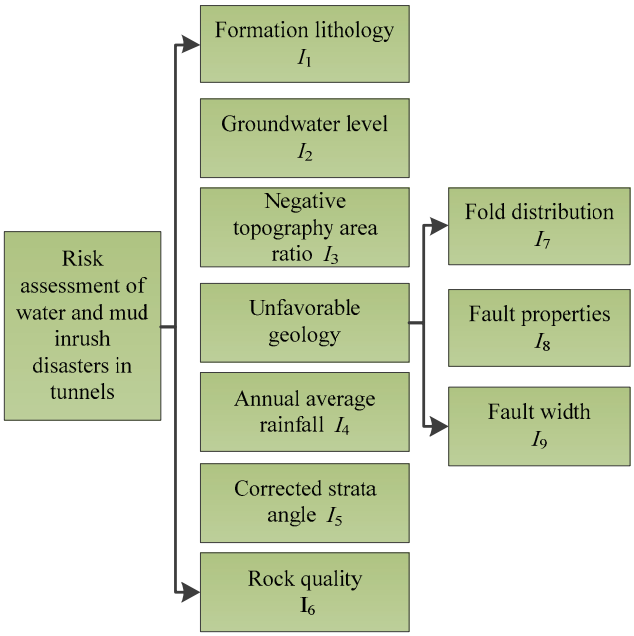

Figure 4. Risk evaluation index system for water inrush disasters in tunnels.

In situ stress was not included as an independent indicator in the present index system. Although in situ stress is important for tunnel stability analysis, the present study focuses on water inrush risk rather than the overall mechanical stability of tunnels. Moreover, consistent in situ stress data were not available for all 20 tunnel cases used for model validation. Therefore, to maintain the consistency and comparability of the evaluation database, in situ stress was not incorporated into the current model as an independent index. Its coupled influence on tunnel water inrush will be further investigated in future studies.

The improved calculation methods of the comprehensive index attribute measure and risk probability were emphasised. The improvement process for the risk attribute interval identification theory for the tunnel water inrush is shown in Figure 5.

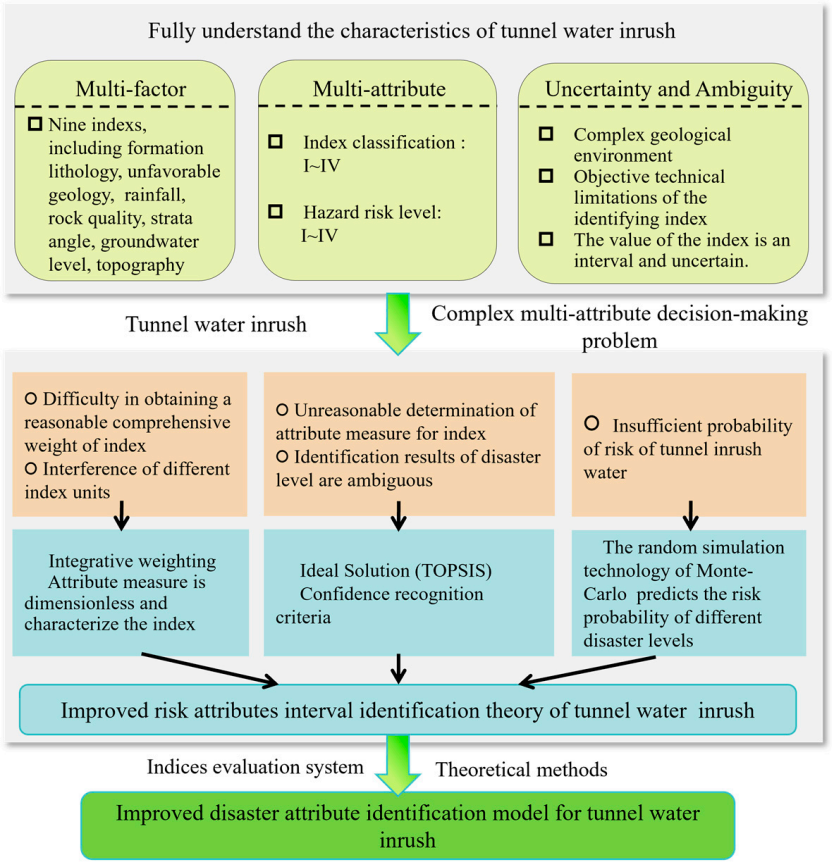

Figure 5. Improvement process for the risk attributes interval identification theory for the tunnel water inrush.

2.2. Attribute Interval Recognition Theory

The number of key factors affecting tunnel water inrush is m, $I_1, I_2, \ldots, I_m$, representing the disaster indices of each factor, respectively. Meanwhile, let F be the risk attribute space for tunnel water inrush, and (C_1, C_2, C_k, …, C_K) is an ordered segmentation class of F. Where C_k is the kth attribute element for water inrush, and $1 \leq k \leq K$. The attribute elements in this ordered segmentation class correspond one-to-one with the risk level of tunnel water inrush, and satisfy $C_1 > C_2 >, \ldots, > C_K$. That is, the risk level corresponding to C_1 is the highest, and the risk level corresponding to C_K is the lowest. According to the value range of each index, corresponding to a type of attribute element, a classification standard matrix would be established, as shown in Equation (1).

$$\begin{array}{c} \\ I_1 \\ I_2 \\ I_3 \\ \vdots \\ I_j \\ \vdots \\ I_9 \end{array} \begin{array}{c} \begin{array}{ccccc} C_1 & C_2 & C_3 & C_k & C_K \end{array} \\ \begin{pmatrix} [a_{11}, b_{11}] & [a_{12}, b_{12}] & [a_{13}, b_{13}] \ldots & [a_{1k}, b_{1k}] \ldots & [a_{1K}, b_{1K}] \\ [a_{21}, b_{21}] & [a_{22}, b_{22}] & [a_{23}, b_{23}] \ldots & [a_{2k}, b_{2k}] \ldots & [a_{2K}, b_{2K}] \\ [a_{31}, b_{31}] & [a_{32}, b_{32}] & [a_{33}, b_{33}] \ldots & [a_{3k}, b_{3k}] \ldots & [a_{3K}, b_{3K}] \\ \vdots & & & & \\ [a_{j1}, b_{j1}] & [a_{j2}, b_{j2}] & [a_{j3}, b_{j3}] \ldots & [a_{jk}, b_{jk}] \ldots & [a_{jK}, b_{jK}] \\ \vdots & & & & \\ [a_{m1}, b_{m1}] & [a_{m2}, b_{m2}] & [a_{m3}, b_{m3}] \ldots & [a_{mk}, b_{mk}] \ldots & [a_{mK}, b_{mK}] \end{pmatrix} \end{array} \quad (1)$$

where a_{jk} and b_{jk} respectively represent the lower and upper limits of the index I_j when corresponding to the attribute C_k. And Equation (1) satisfies that $a_{jk} \leq b_{jk}$, $a_{j1} > a_{j2} > a_{j3} > \ldots a_{jk} \ldots > a_{jK}$ and $b_{j1} > b_{j2} > b_{j3} > \ldots b_{jk} \ldots > b_{jK}$.

The testing result of the j_{th} index I_j is denoted as x_j, and satisfies that $1 \leq j \leq m$. The attribute measure interval with the attribute C_k is denoted as $\mu_{jk} = \left[\underline{\mu}_{jk}, \overline{\mu}_{jk}\right]$. Where the $\underline{\mu}_{jk}$ is the lower limiting value of the attribute measure of the index I_j, and the $\overline{\mu}_{jk}$ is the upper limiting value of the attribute measure of the index I_j. The calculation for the attribute measure interval of the index I_j is as follows:

(1) when $x_j \geq a_{j,1}$, $\underline{\mu}_{j1} = 1$, $\underline{\mu}_{j1} = \ldots = \underline{\mu}_{jK} = 0$;

(2) when $x_j \geq b_{j,1}$, $\overline{\mu}_{j1} = 1$, $\overline{\mu}_{j1} = \ldots \overline{\mu}_{jK} = 0$;

(3) when $x_j \leq a_{j,4}$, $\underline{\mu}_{j,K} = 1$, $\underline{\mu}_{j,1} = \ldots = \underline{\mu}_{j,K-1} = 0$;

(4) when $x_j \leq b_{j,4}$, $\overline{\mu}_{j,K} = 1$, $\overline{\mu}_{j,1} = \ldots \overline{\mu}_{j,K-1} = 0$;

(5) when $a_{j,l+1} \leq x_j \leq a_{j,l}$, $\underline{\mu}_{j,l} = \left|\frac{x_j - a_{j,l+1}}{a_{j,l} - a_{j,l+1}}\right|$, $\underline{\mu}_{j,l+1} = \left|\frac{x_j - a_{j,l}}{a_{j,l} - a_{j,l+1}}\right|$, $\underline{\mu}_{j,k} = 0$;

(6) when $b_{j,l+1} \leq x_j \leq b_{j,l}$, $\overline{\mu}_{j,l} = \left|\frac{x_j - b_{j,l+1}}{b_{j,l} - b_{j,l+1}}\right|$, $\overline{\mu}_{j,l+1} = \left|\frac{x_j - b_{j,l}}{b_{j,l} - b_{j,l+1}}\right|$, $\overline{\mu}_{j,k} = 0$;

Where $k < l$ or $k < l + 1$.

2.3. Integrative Weighting Based on the AHP-IEM-GT

Due to the fuzziness and uncertainty characteristics of water inrush in tunnels, the calculation methods for the index weights can be divided into subjective weight and objective weight. Subjective weights rely on expert experience to determine, such as the commonly used AHP [42]. The objective weight depends on the statistical analysis of the measured data, which is limited by the reliability of the measured results, such as the commonly used entropy weight method and IEM. Compared to the entropy weight method, the IEM is less affected by differences in indices [43]. To obtain reasonable values for the indices' weights, it is often necessary to perform a combination of subjective and objective weighting. GT can minimise the final weight deviation by linearly combining the weights obtained by different weighting methods and can simultaneously reflect subjective and objective information and coordinate the differences between the two [44]. Therefore, the present study used AHP to determine the subjective weights of indices, and the objective weights of disaster indicators were determined using the IEM. Finally, GT was introduced to achieve a combination of subjective and objective weighting. The specific steps are as follows.

Step 1. The '1–9' scaling method was used to establish the judgement matrix A, as shown in Equation (2).

$$A = (a_{ij})_{m \times m} \tag{2}$$

where a_{ij} represents the degree of impact of I_i and I_j on water inrush, and the calculation standard is shown in Table 2. The judgement matrix satisfies $a_{ij} > 0$, $a_{ji} = 1/a_{ij}$, and $a_{ii} = 1$. m represents the dimension of the judgement matrix for the disaster indices.

Table 2. Calculation standard for the scale of the indices.

Scale	Value Principle
1	I_i and I_j have the same importance.
3	I_i is slightly more important than the I_j.
5	I_i is significantly more important than the I_j.
7	I_i is more strongly important than the I_j.
9	I_i is extremely more important than the I_j.
2, 4, 6, 8	The median of the adjacent judgement results mentioned above.
Others	The I_j value is taken as the reciprocal of the above evaluation results.

Step 2. The maximum eigenvalue λ_{max} and corresponding eigenvector w of the judgement matrix were calculated, and the consistency of the judgement matrix was checked using the AHP consistency ratio method, as shown in Equation (3) [42].

$$\left.\begin{array}{l} C.I. = \frac{\lambda_{\max} - m}{m-1} \\ C.R. = \frac{C.I.}{R.I.} \end{array}\right\} \quad (3)$$

where *C.I.* is the criterion for determining matrix consistency, *R.I.* represents the average random consistency index of the judgement matrix, and the value standard is listed in Table 3.

Table 3. Value standard for the average random consistency index R.I.

Dimension of the Matrix	**1**	**2**	**3**	**4**	**5**	**6**
R.I.	0	0	0.52	0.89	1.12	1.26
Dimension of the Matrix	**7**	**8**	**9**	**10**	**11**	**12**
R.I.	1.36	1.41	1.46	1.49	1.52	1.54

Step 3. When C.R. < 0.1, the consistency requirement of the judgement matrix was met. The w was normalised to obtain the subjective weight vector, as shown in Equation (4).

$$w' = \begin{bmatrix} w_{11} & w_{21} & \cdots & w_{m1} \end{bmatrix} \quad (4)$$

Step 4. The measured data of tunnel water inrush can be obtained through case studies. The number of indices is m. The matrix of measured data for tunnel water inrush would be established, as shown in Equation (5).

$$X = (x_{ij})_{n\times m} = \begin{pmatrix} x_{11} & x_{12} & x_{13} & \cdots & x_{1m} \\ x_{21} & x_{22} & x_{23} & \cdots & x_{2m} \\ x_{31} & x_{32} & x_{33} & \cdots & x_{3m} \\ \vdots & & & & \\ x_{n1} & x_{n2} & x_{n3} & \cdots & x_{nm} \end{pmatrix} \quad (5)$$

where x_{ij} represents the j_{th} index for the i_{th} measured data, i = 1, 2, 3, …, n, and j = 1, 2, 3, …, m.

Step 5. The matrix X was standardised. The objective weights can be obtained by combining Equations (6) and (7), as shown in Equation (8).

$$e_j = -\sum_{i=1}^{n} \left(t_{ij} In\left(1 - t_{ij}\right)\right) \quad (6)$$

$$w_j = -\frac{e_j}{\sum_{j=1}^{m} e_j} \quad (7)$$

where $t_{ij} = \frac{y_{ij}}{\sum_{i=1}^{n} y_{ij}}$ and y_{ij} is standardised data.

$$w'' = \begin{bmatrix} w_{12} & w_{22} & \cdots & w_{m2} \end{bmatrix} \quad (8)$$

Step 6. Consistency testing was performed on Equations (4) and (8) using Equation (9).

$$d\left(\omega_j', \omega_j''\right) = \sqrt{\frac{1}{2}\sum_{j=1}^{m}\left(\omega_j' - \omega_j''\right)^2} \tag{9}$$

where $d\left(\omega_j', \omega_j''\right)$ is the distance between Equations (4) and (8). When $0 \leq d \leq 1$, the consistency requirement is met.

Step 7. The combination form of subjective and objective weight vectors is shown in Equation (10).

$$w = \theta_1\left(w_j'\right)^T + \theta_2\left(w_j''\right)^T \tag{10}$$

where w is the combination weighting, θ_1 and θ_2 are the combination coefficients.

Step 8. The objective function F (θ_1, θ_2) was constructed by minimising the deviation, as shown in Equation (11).

$$F(\theta_1, \theta_2) = \min\left\|\omega - \widetilde{\omega}_\eta\right\|, \eta = 1, 2 \tag{11}$$

where $\widetilde{\omega}_\eta = \left[\omega_j' \; \omega_j''\right]$.

Step 9. The values of θ_1 and θ_2 were calculated by finding the first-order derivative of Equation (11), as shown in Equation (12).

$$\left.\begin{array}{l} \widetilde{\theta}_1 = \frac{\theta_1}{\theta_1+\theta_2} \\ \widetilde{\theta}_2 = \frac{\theta_2}{\theta_1+\theta_2} \end{array}\right\} \tag{12}$$

where $\widetilde{\theta}_1$ and $\widetilde{\theta}_2$ are the normalised combination coefficients.

Step 10. The combined weight vector would be obtained by substituting Equation (12) into Equation (10) and normalising, as shown in Equation (13).

$$w = \{w_j\} = \{w_1, w_2, w_3, w_4, \ldots w_9\} \tag{13}$$

where $w_j > 0$, $j = 1, 2, \ldots, 9$, $\sum_{j=1}^{9} w_j = 1$.

2.4. Analysis of Disaster Indices Attributes Measure Based on TOPSIS

For the measured result $x_j = \{x_1, x_2, x_3, \ldots, x_m\}$, the specific steps for calculating the comprehensive index attribute measure based on the TOPSIS are as follows:

Step 1. The TOPSIS theory holds that the positive ideal solution is the maximum value of the index, and the negative ideal solution is the minimum value of the index. Combining Equation (1), the positive ideal point matrix and inverse ideal point matrix of the tunnel water inrush were determined, as shown in Equations (14) and (15).

$$F^*(+) = \begin{pmatrix} b_{11} & b_{12} & b_{13} & \ldots & b_{1K} \\ b_{21} & b_{22} & b_{23} & \ldots & b_{2K} \\ b_{31} & b_{32} & b_{33} & \ldots & b_{3K} \\ \vdots & & & & \\ b_{m1} & b_{m2} & b_{m3} & \ldots & b_{mK} \end{pmatrix} \tag{14}$$

$$F^*(-) = \begin{pmatrix} a_{11} & a_{12} & a_{13} & \dots & a_{1K} \\ a_{21} & a_{22} & a_{23} & \dots & a_{2K} \\ a_{31} & a_{32} & a_{33} & \dots & a_{3K} \\ \vdots & & & & \\ a_{m1} & a_{m2} & a_{m3} & \dots & a_{mK} \end{pmatrix} \quad (15)$$

Step 2. For any measured result x_j, the Euclidean distance method was used to calculate the distances between the measured result and the positive ideal point and the inverse ideal point, which are denoted as D_{1k} and D_{2k}, as shown in Equation (16).

$$\left.\begin{aligned} D_{1k} &= \sqrt{\sum_{j=1}^{m} w_j \left(\frac{x_j - b_{jk}}{b_{jk}}\right)^2} \\ D_{2k} &= \sqrt{\sum_{j=1}^{m} w_j \left(\frac{x_j - a_{jk}}{a_{jk}}\right)^2} \end{aligned}\right\} \quad (16)$$

where $j = 1, 2, 3, \dots, m$; $k = 1, 2, 3, \dots, K$.

Step 3. The ideal point closeness, T_k, was calculated. Let $\alpha_k = T_k$, and the comprehensive attribute measure would be determined, as shown in Equation (17).

$$\mu'_{jk} = \alpha_k \cdot \underline{\mu}'_{jk} + (1 - \alpha_k) \cdot \overline{\mu}'_{jk} \quad (17)$$

where α_k is the index attribute measure coefficient, and $\alpha_k = T_k = \frac{D_{2k}}{D_{1k}+D_{2k}}$.

2.5. Risk Attribute Identification of Tunnel Water Inrush

(1) Risk attribute identification

The risk attribute identification of tunnel water inrush was implemented using the minimum confidence criterion, which has been widely applied in attribute recognition and attribute interval recognition methods, as shown in Equation (18) [36,40].

$$k_0 = \min\left\{k : \sum_{i=1}^{k} \mu_{x_i}(C_{k_i}) \geq \lambda, 1 \leq k \leq K\right\} \quad (18)$$

where C_{ki} is the risk attribute corresponding to the measured result x_i; λ is the confidence level, usually ranging between 0.6 and 0.7.

(2) Risk probability identification

Due to the complexity of topographic and geological conditions, the measured results of the disaster index are usually within an interval. To obtain the risk probability of tunnel water inrush, a random number β was introduced to construct the possible value of disaster indices, as shown in Equation (19).

$$z_j = x_j + \beta(y_j - x_j) \quad (19)$$

where $x_j \leq y_j$, $j = 1, 2, \dots, m$; $0 < \beta < 1$.

By combining Equation (19) and using the Monte Carlo strategy, sets of values of disaster indices within the measured interval would be obtained. For any disaster index value, the k_0 value and corresponding risk attribute would be calculated. The risk probability of tunnel water inrush would be obtained by counting the evaluation results.

(3) Identification process of risk level for tunnel water inrush

Step 1. For measured results $\left[\vec{x}_j, \vec{y}_j\right]$, 1000 random numbers within the range of 0 to 1 were first generated. To ensure the uniqueness of the selected random numbers, the 0–1 interval was evenly divided into 1000 small intervals, and a value was randomly taken in each small interval to establish a vector containing 1000 random numbers. Then, according to Equation (19), 1000 values of the evaluation index were constructed that conform to the range of the index.

Step 2. For each index value, the index attribute measure interval was determined according to the method in Section 2.2.

Step 3. The index attribute measure coefficient was determined using the method described in Section 2.4. According to Equation (19), the attribute measures corresponding to different attribute levels would be determined. Furthermore, the risk level assessment would be completed based on the principle of minimum confidence.

Step 4. The risk identification results of 1000 times would be obtained by repeating steps 2 and 3. Furthermore, the risk probability would be obtained by calculating the frequency of occurrence of each disaster risk level. The risk identification process for tunnel water inrush is shown in Figure 6.

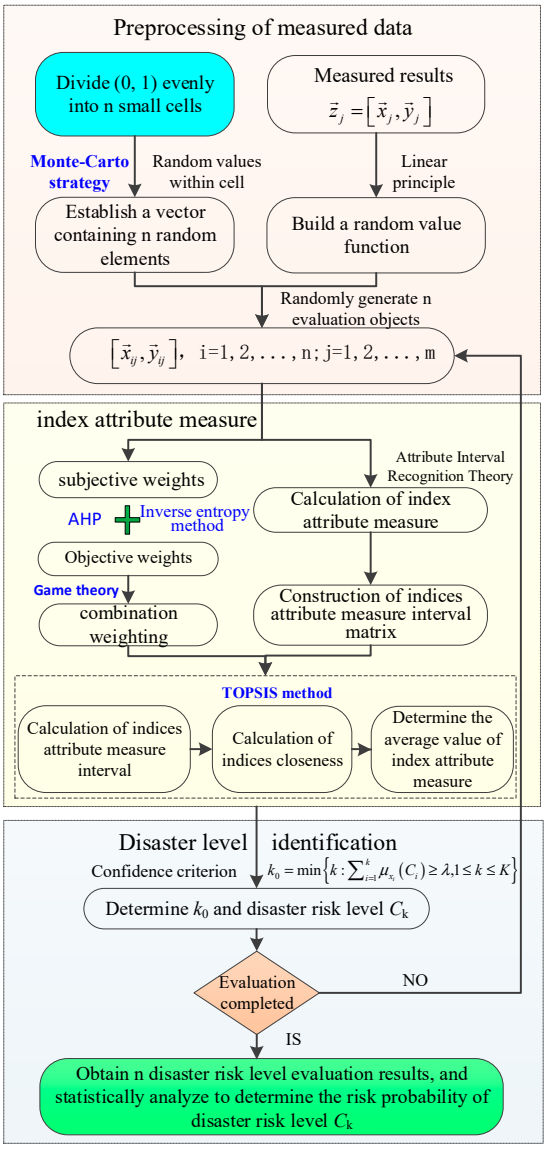

Figure 6. Identification process of the tunnel water inrush.

3. Case Study

3.1. Project Overview and Geological Conditions

The Nafeng Water Conveyance Tunnel, which is under the administration of Nanning City, Guangxi, mainly links the Fengtinghe Reservoir with the Naban Reservoir. It protects the water supply security of towns like Nanning and Qinzhou, and it is a key project for the best distribution of water resources in the Beibu Gulf Rim. A free-flow water conveyance system with a horseshoe-shaped cross-section is used in the Nafeng Tunnel. The tunnel is built using the drill-and-blast method, and its net cross-sectional dimensions (Width × Height) are 3 m × 3.8 m. With a total length of 8.865 kilometres, the Nafeng Main Line mostly passes through rough landscapes. The inlet's invert elevation is 195 m. As shown in Figure 7, the ground elevation along the alignment varies between 230 and 517 m, whereas the burial depth varies between 4 and 236 m.

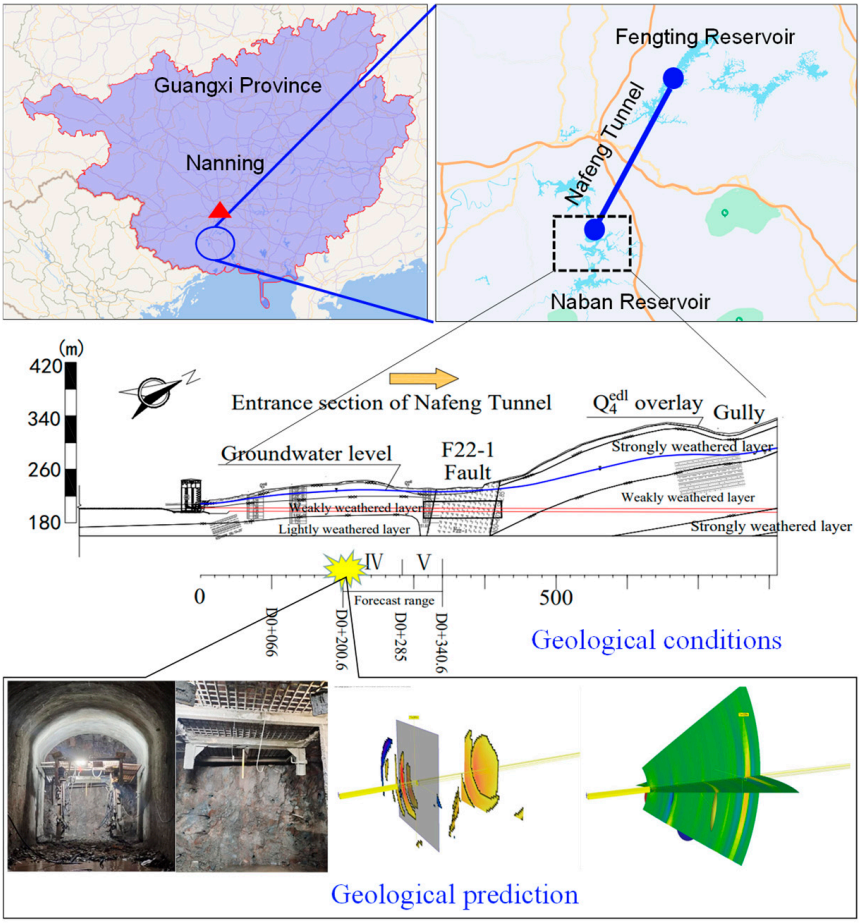

Figure 7. Geological conditions of the entrance section of Nafeng Tunnel. Note: The triangle indicates the location of Nanning City, Guangxi Province. IV and V denote Class IV and Class V surrounding rock, respectively.

The geological and hydrogeological conditions of the entrance section were compiled from preliminary investigation, design documents, tunnel-face exposure, and advanced geophysical prediction. The key results are summarised in Table 4. Overall, the evaluated section D0 + 220.6–D0 + 340.6 m is characterised by developed fissures and abundant groundwater, while the second subsection is directly affected by the F22-1 fault fracture zone. Therefore, this section was selected for detailed water inrush risk assessment and was divided into two subsections, D0 + 220.6–D0 + 285 m and D0 + 285–D0 + 340.6 m, according to the surrounding-rock classification and the influence of the F22-1 fault fracture zone.

Table 4. Summary of geological and hydrogeological conditions of the entrance section of the Nafeng Tunnel.

Data Source/Section	Preliminary Investigation: D0 + 066–D0 + 300 m	Preliminary Investigation: D0 + 300–D0 + 498 m	Advanced Geophysical Prediction: D0 + 220.6–D0 + 340.6 m
Topography and tunnel geometry	Slightly undulating terrain; ground elevation: 224–254 m; burial depth: 22–52 m.	Slightly undulating terrain; ground elevation: 244–290 m; burial depth: 43–89 m.	Prediction conducted at the tunnel face of D0 + 220.6 on 11 May 2025; prediction range: 120 m ahead of the face, covering D0 + 220.6–D0 + 340.6 m.
Lithology and rock-mass condition	Lower Member of the Baixing Formation, Lower Jurassic system; interbedded medium-thick silty mudstone and argillaceous siltstone, locally intercalated with sandstone, with an approximate ratio of 4:4:1. The rock mass is weakly weathered, with integrity ranging from poor to relatively intact. Surrounding rock: Class IV (60%) and Class V (40%).	Strongly weathered sandstone intercalated with silty mudstone. The rock mass is broken or highly fractured. Surrounding rock: Class V.	The rock mass at the tunnel face is mainly medium-thick to thick-bedded argillaceous siltstone, intercalated with minor thin-bedded fine sandstone. The rock mass is weakly weathered and broken. Tunnel-face exposure indicates Class IV–V surrounding rock.
Hydrogeological and structural characteristics	Intersection angle between rock strike and tunnel axis: 60–90°; strata dip angle: 10–20°. The tunnel body is located below the groundwater table.	The F22-1 fault fracture zone is developed within D0 + 325–D0 + 413 m, with a width of approximately 88 m. The zone is characterised as a rock-debris-with-mud type and is mainly composed of strongly weathered sandstone, argillaceous siltstone, and silty mudstone. The material has poor cementation and contains confined water.	Strata dip angle at the face: 21°. Steeply dipping joints are developed, with dip angles of 60–75°, apertures of 0.5–3 mm, and spacing of 0.2–0.4 m. The joints are unfilled or filled with argillaceous-calcareous material and contain fissure water.
Implication for water inrush risk	The relatively poor surrounding-rock quality and groundwater conditions indicate a potential water inrush risk.	The F22-1 fault fracture zone may act as a major water-conducting pathway and poses a significant water inrush risk.	The predicted section contains fractured rock mass, water-bearing fissures, and adverse structural conditions, indicating increased susceptibility to water inrush.

3.2. Risk Factor Analysis and Model-Input Preparation

Based on the geological and hydrogeological conditions summarised in Section 3.1, the section D0 + 220.6–D0 + 340.6 m was selected for detailed water inrush risk assessment. This section was divided into two subsections, D0 + 220.6–D0 + 285 m and D0 + 285–D0 + 340.6 m, according to the surrounding-rock classification and the influence of the F22-1 fault fracture zone. The first subsection is located before the main F22-1 fault fracture zone. Although no direct fault exposure was identified in this subsection, it is affected by the nearby F22-1 fault. The second subsection intersects the F22-1 fault fracture zone and is characterised by broken surrounding-rock, abundant groundwater, and confined water-bearing conditions.

To apply the proposed hybrid model to the Nafeng Tunnel, the site-specific geological information was converted into nine assessment indices: formation lithology, groundwater level, negative topography area ratio, annual average rainfall, corrected strata angle, rock quality, fold distribution, fault properties, and fault width. These indices correspond to

the seven factor categories established in Section 2.1 and provide the model inputs for risk level identification and probability estimation.

The classification criteria used for the nine assessment indices were compiled and adapted from previous studies on tunnel water inrush risk assessment [40,45–49]. These studies provide the basis for grading the main geological, hydrogeological, geomorphological, and structural factors considered in this study. The classification criteria for the nine assessment indices are shown in Table 5.

Table 5. Classification criteria for risk assessment indices of water inrush in tunnels [40,45–49].

Disaster Indicators	I (Extremely)	II (High)	III (Medium)	IV (Low)
Formation lithology (I_1)	0.254~0.636	0.104~0.254	0.042~0.104	0~0.042
Groundwater level/m (I_2)	60~90	30~60	10~30	0~10
Negative topography area ratio (I_3)	60~100	40~60	20~40	0~20
Annual average rainfall/mm (I_4)	1200~2250	1100~1200	1000~1100	600~1000
Corrected strata angle/° (I_5)	25~45	10~25	5~10	0~5
Rock quality (I_6)	IV, V (80~100)	III (50~80)	II (20~50)	I (0~20)
Folds distribution (I_7)	Nucleus of folds (80~100)	Wings of wrinkle (50~80)	Monocline (20~50)	Weak (0~20)
Fault properties (I_8)	Tension (80~100)	Tension torsion (50~80)	Torsional (20~50)	Compressive (0~20)
Fault width/m (I_9)	10~35	2~10	1~2	0~1

To clarify the physical meaning of the geomorphological indicator, the negative topography area ratio (I_3) was interpreted as the proportion of closed negative landforms within the surface catchment or influence area above the evaluated tunnel section. A conceptual illustration of this indicator is provided in Figure 8.

$$I_3 = \frac{A_{nt}}{A_t} \times 100\% \tag{20}$$

where A_{nt} denotes the area of closed negative landforms, such as depressions, trough valleys, sinkholes, or other low-lying catchment zones, and A_t denotes the total surface catchment or influence area considered for the evaluated tunnel section. A larger I_3 indicates stronger surface-water convergence and groundwater recharge potential, which may increase the susceptibility to tunnel water inrush.

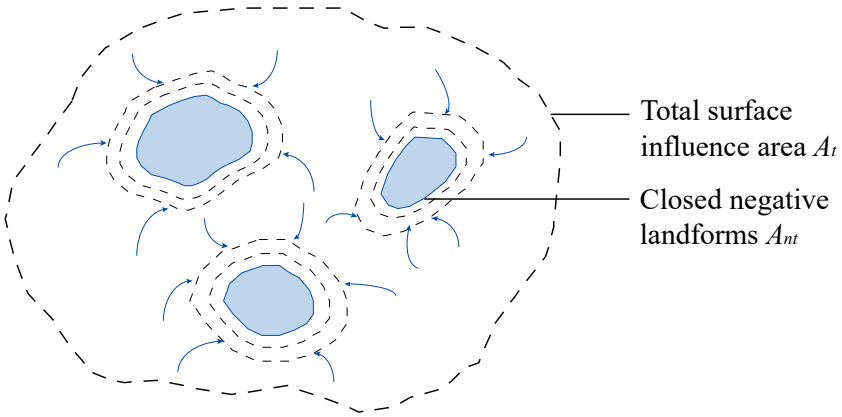

Figure 8. Conceptual illustration of the negative topography area ratio. Note: The arrow indicates the direction of surface runoff or groundwater recharge toward the closed negative landform.

Among these indices, the strata angle was characterised by the corrected strata angle, as shown in Table 6.

Table 6. Classification of the corrected strata angle [40].

Risk Level	Strata Angle φ/°	Correction Formula	Corrected Strata Angle φ'/°
I (Extremely)	$25^\circ \le \varphi < 45^\circ$ $45^\circ \le \varphi \le 65^\circ$	$\varphi' = \varphi$ $\varphi' = 25 + (65 - \varphi)$	$25^\circ \le \varphi^\circ < 45^\circ$
II (High)	$10^\circ \le \varphi < 25^\circ$ $65^\circ < \varphi < 85^\circ$	$\varphi' = \varphi$ $\varphi' = 10 + (80 - \varphi)$	$10^\circ \le \varphi^\circ < 25^\circ$
III (Medium)	$80^\circ < \varphi \le 90^\circ$	$\varphi' = 5 + (90 - \varphi)/2$	$5^\circ \le \varphi^\circ < 10^\circ$
IV (Low)	$0^\circ \le \varphi < 10^\circ$	$\varphi' = \varphi/2$	$0^\circ \le \varphi^\circ < 5^\circ$

To further clarify the input data used in the Nafeng Tunnel risk assessment, the selected values or ranges of the nine assessment indices were summarised according to the seven factor categories, as shown in Table 7. The values were determined from geological investigation, design documents, advanced geophysical prediction, tunnel-face exposure, and the classification criteria adopted in this study. For continuous indicators, the measured or interpreted ranges were used as input uncertainty intervals in the attribute interval recognition and Monte Carlo procedures. For categorical indicators, such as formation lithology, rock quality, fold distribution, and fault properties, conventional statistical margins of error were not available; therefore, their uncertainty was represented by the corresponding classification category or interval in Table 5. Through this procedure, the descriptive field information of the Nafeng Tunnel was transformed into standardised quantitative or semi-quantitative inputs for the proposed hybrid risk assessment model.

Table 7. Input values and selection basis of the assessment indices for the Nafeng Tunnel.

Factor Category	Indicator	D0 + 220.6–D0 + 285 m	D0 + 285–D0 + 340.6 m	Basis for Selection
Formation lithology	Formation lithology (I_1)	t = 0	t = 0	Argillaceous siltstone and sandstone; non-soluble strata
Groundwater condition	Groundwater level/m (I_2)	31.62–32.37 m	29.70–30.66 m	Hydraulic head difference between the groundwater level and the tunnel invert
Topography	Negative topography area ratio (I_3)	0%	0–20%	Geomorphological interpretation based on the definition in Equation (20) and Figure 8
Rainfall	Annual average rainfall/mm (I_4)	1715 mm	1715 mm	Regional mean annual precipitation from meteorological or design data

Table 7. *Cont.*

Factor Category	Indicator	D0 + 220.6–D0 + 285 m	D0 + 285–D0 + 340.6 m	Basis for Selection
Strata attitude	Corrected strata angle/° (I_5)	10–20°	10–20°	Geological survey results and correction rule in Table 6
Rock quality	Rock quality (I_6)	Class IV	Class V	Tunnel-face exposure and surrounding-rock classification
Unfavourable geological conditions	Folds distribution (I_7)	Fold wing	Fold wing	Geological structural interpretation
Unfavourable geological conditions	Fault properties (I_8)	Influenced by F22-1	Influenced by F22-1	Geological survey and advanced prediction
Unfavourable geological conditions	Fault width/m (I_9)	0 m	88 m	The first subsection does not directly intersect the fault zone; the second subsection intersects the F22-1 fault fracture zone

For the second subsection, the interpreted width of the F22-1 fault fracture zone is approximately 88 m, which exceeds the highest-risk threshold of the fault-width indicator in Table 5. Therefore, this indicator was assigned to the highest-risk interval in the model. For the first subsection, no direct fault exposure was identified; therefore, the fault-width indicator was assigned as 0 m, while the influence of the nearby F22-1 fault was considered in the integrated geological interpretation.

Based on the classification criteria in Table 5 and the input values in Table 7, the attribute interval matrix of tunnel water inrush was constructed, as shown in Equation (21).

$$\begin{array}{c} \\ I_1 \\ I_2 \\ I_3 \\ I_4 \\ I_5 \\ I_6 \\ I_7 \\ I_8 \\ I_9 \end{array} \begin{array}{c} \begin{array}{cccc} C_1 & C_2 & C_3 & C_4 \end{array} \\ \left(\begin{array}{cccc} [0.254, 0.636] & [0.104, 0.254] & [0.042, 0.104] & [0, 0.042] \\ [60, 90] & [30, 60] & [10, 30] & [0, 10] \\ [60, 100] & [40, 60] & [20, 40] & [0, 20] \\ [1200, 2250] & [1100, 1200] & [1000, 1100] & [600, 1000] \\ [25, 45] & [10, 25] & [5, 10] & [0, 5] \\ [80, 100] & [50, 80] & [20, 50] & [0, 20] \\ [80, 100] & [50, 80] & [20, 50] & [0, 20] \\ [80, 100] & [50, 80] & [20, 50] & [0, 20] \\ [10, 35] & [2, 10] & [1, 2] & [0, 1] \end{array} \right) \end{array} \quad (21)$$

4. Results and Discussion

4.1. Index Attribute Measures

The attribute measure interval functions for the nine water inrush indices would be determined using Equation (21) and the attribute measure interval calculation method for disaster indices in Section 2.2, as illustrated in Figure 9.

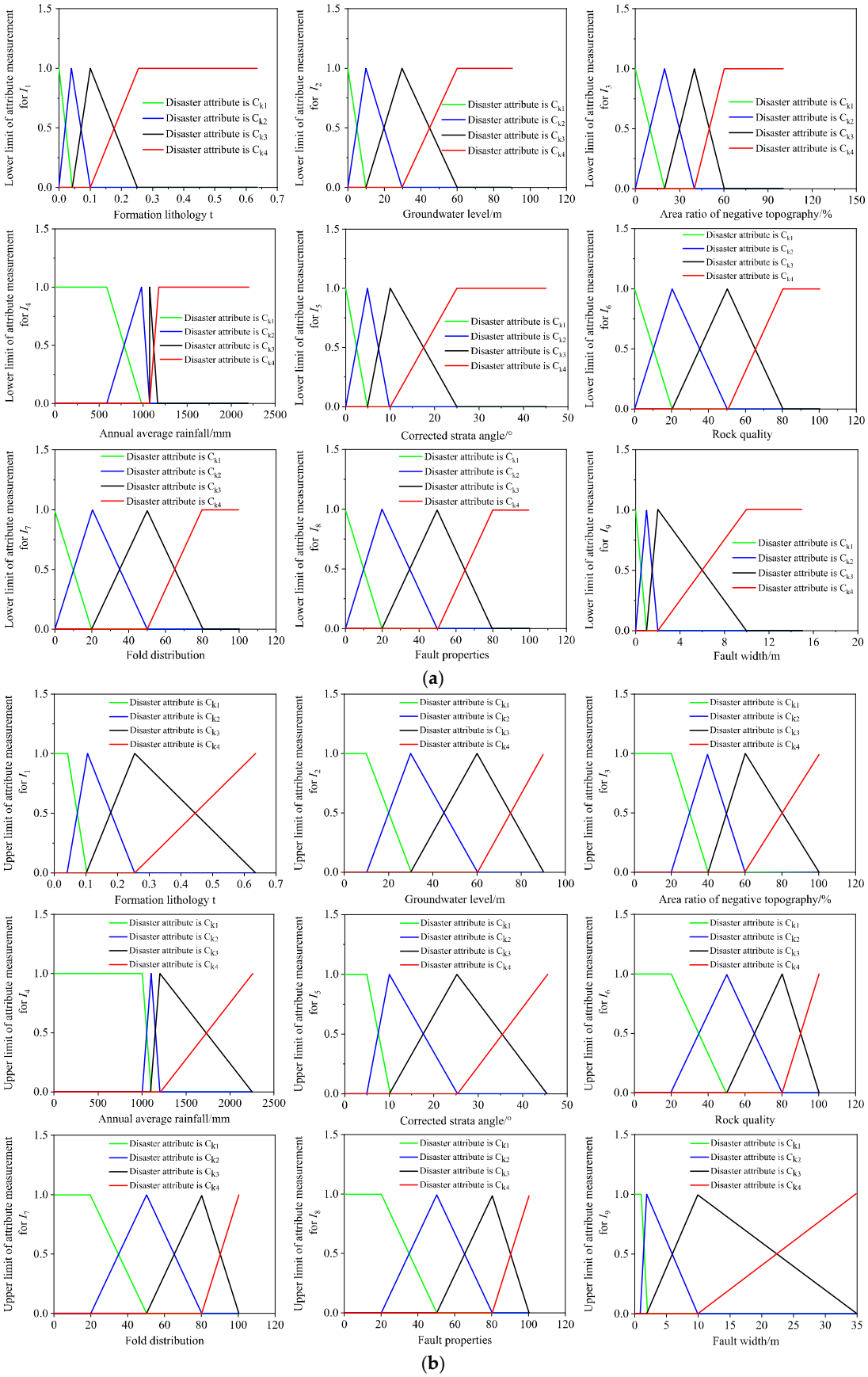

Figure 9. Index attribute measure: (**a**) lower limit; (**b**) upper limit.

4.2. Combination Weights

Using the AHP method and combining with the research results of Xu et al. [45], nine indicators, including formation lithology, groundwater level, negative topography area ratio, corrected strata angle, rock quality, annual average rainfall, fold distribution, fault properties, and fault width, were valued. The index judgement matrix for tunnel water inrush was established, as shown in Equation (22).

$$A = \begin{bmatrix} 1 & 1 & 2 & 2 & 3 & 4 & \frac{1}{2} & \frac{1}{2} & 2 \\ 1 & 1 & 2 & 2 & 3 & 4 & \frac{1}{2} & \frac{1}{2} & 2 \\ \frac{1}{2} & \frac{1}{2} & 1 & 1 & 2 & 3 & \frac{1}{4} & \frac{1}{4} & 1 \\ \frac{1}{2} & \frac{1}{2} & 1 & 1 & 2 & 3 & \frac{1}{4} & \frac{1}{4} & 1 \\ \frac{1}{3} & \frac{1}{3} & \frac{1}{2} & \frac{1}{2} & 1 & 2 & \frac{1}{6} & \frac{1}{6} & \frac{1}{2} \\ \frac{1}{4} & \frac{1}{4} & \frac{1}{3} & \frac{1}{3} & \frac{1}{2} & 1 & \frac{1}{7} & \frac{1}{7} & 1 \\ 2 & 2 & 4 & 4 & 6 & 7 & 1 & 1 & \frac{1}{4} \\ 2 & 2 & 4 & 4 & 6 & 7 & 1 & 1 & \frac{1}{4} \\ \frac{1}{2} & \frac{1}{2} & 1 & 1 & 2 & 1 & 4 & 4 & 1 \end{bmatrix} \quad (22)$$

Based on Section 2.3, the maximum feature value of the matrix A is 7.0525. The value of the consistency judgement index CR is 0.0508, which is less than 0.1. The judgement matrix A met the consistency requirement. By normalising the feature vectors, the comprehensive weights of the indices were shown in Equation (23).

$$\omega_{subjective} = [0.1779, 0.1779, 0.0985, 0.0985, 0.0583, 0.0386, 0.1578, 0.154, 0.0385]^T \quad (23)$$

The IEM was used to analyse the measured case. Taking into account the research findings of Zhou et al. [40] and Li et al. [46], the objective weight of the tunnel water inrush indices was determined as shown in Equation (24).

$$\omega_{objective} = [0.166, 0.185, 0.102, 0.069, 0.042, 0.062, 0.186, 0.12, 0.068]^T \quad (24)$$

Using GT to optimise the combination of subjective and objective weights, the distance between the subjective and objective weight vectors is 0.0485, satisfying the consistency condition. The results show that the subjective weight proportion is 0.6942 and the objective weight proportion is 0.3058. The combined weight vector was shown in Equation (25).

$$\omega = [0.1743, 0.1801, 0.0996, 0.0895, 0.0533, 0.0458, 0.1664, 0.1436, 0.0475] \quad (25)$$

4.3. Reliability of the Model

To further verify the effectiveness of the present model, typical tunnel water inrush disaster cases were selected with the selection principle that includes all risk levels to carry out risk level prediction and comparative analysis. Relevant data were derived from existing research findings [2,5,6,35,46–49], including the Yesanguan tunnel, Bieyancao tunnel, Qiyue Mountain tunnel of Yiwan Railway, Jigongling tunnel, and so on. A total of 20 typical tunnel engineering water inrush disaster cases were selected, including 8 cases of Class I risk level, 9 cases of Class II risk level, 2 cases of Class III risk level, and 1 case of Class IV risk level. Among them, the two cases of DK268 + 725~825 in the Lianhuashan tunnel and the No. 2 inclined shaft in the Maiji Mountain tunnel of Pumei Railway are fault-type water inrush structures, while the rest are mainly karst-type water inrush structures. To provide more detailed information on the validation database, the key characteristics of the 20 cases are summarised in Table 8, and their geographic distribution is shown in Figure 10.

Table 8. Key characteristics of the 20 tunnels water inrush cases used for model validation.

No.	Tunnel/Section	Location	Inrush Characteristics and Associated Geological Condition	Actual Risk Level
1	Yesanguan Tunnel DK124 + 602	Badong County, Hubei Province, China	Water and mud/rock inrush associated with a karst cave and a water-rich fault zone	I
2	Dongquan Tunnel	Tongjing Town, Chongqing, China	Water inrush associated with water-bearing karst structures	I
3	Bieyancao Tunnel	Shuangliu Township, Chongqing, China	Fault-related water inrush associated with the F3 fault fracture zone	I
4	Wuzhishan Tunnel K30 + 680~750	Heping County, Guangdong Province, China	Karst-related water inrush associated with karst development and water-bearing karst structures	I
5	Dayaoshan Tunnel DK1911 + 382~395	Shaoguan City, Guangdong Province, China	High-pressure water inrush associated with fractured sandstone and water-bearing fractured zones	I
6	Jinzishan Tunnel	Zhongshan City, Guangdong Province, China	Karst-related water and mud inrush associated with filled karst cavities or water-bearing karst structures	I
7	Tianchi Tunnel	Chongqing, China	Karst-related water inrush associated with water-bearing karst structures	I
8	Longtan Tunnel	Changyang County, Hubei Province, China	Karst-related water and mud inrush associated with karst fissures and conduit systems	I
9	Qiyueshan Tunnel DK364 + 005	Lichuan City, Hubei Province, China	Karst water inrush associated with a karst fissure network and karst groundwater system	II
10	Qiyueshan Tunnel PDK365 + 313	Lichuan City, Hubei Province, China	Water and sand/rock inrush associated with a high-pressure water-bearing fault zone	II
11	Jijiapo Tunnel	Sandouping Town, Yichang City, Hubei Province, China	Karst-related water inrush associated with steeply inclined filled karst fissures	II
12	Lianhuashan Tunnel DK268 + 725~825	Jiangmen City, Guangdong Province, China	Fault-type water inrush associated with a fault fracture zone	II
13	Wuzhishan Tunnel K29 + 542	Heping County, Guangdong Province, China	Fault-related water inrush associated with a fault fracture zone	II
14	Yuelongmen Tunnel	Mianyang–Aba area, Sichuan Province, China	Water inrush associated with active faults, fractured zones, and karst water	II
15	Jigongling Tunnel ZK19 + 509	Yichang City, Hubei Province, China	Karst-related water inrush associated with water-bearing karst structures	II

Table 8. *Cont.*

No.	Tunnel/Section	Location	Inrush Characteristics and Associated Geological Condition	Actual Risk Level
16	Tongluoshan Tunnel K33 + 940~K34 + 035	Linshui County, Guang'an City, Sichuan Province, China	Water inrush associated with karst and fractured water-bearing structures	II
17	Binghui Tunnel DK353 + 510~540	Yiliang County, Zhaotong City, Yunnan Province, China	Water inrush associated with faults, folds, and water-bearing geological structures	II
18	Tanchang Tunnel YK27 + 235	Northern Guizhou Province, China	Karst-related water inrush associated with water-bearing karst structures	III
19	Pingan Tunnel	Aba Tibetan and Qiang Autonomous Prefecture, Sichuan Province, China	Water and mud inrush associated with water-bearing fractured or karst structures	III
20	Maijishan Tunnel	Tianshui City, Gansu Province, China	Fault-type water inrush associated with a fault fracture zone and water-rich fractured rock mass	IV

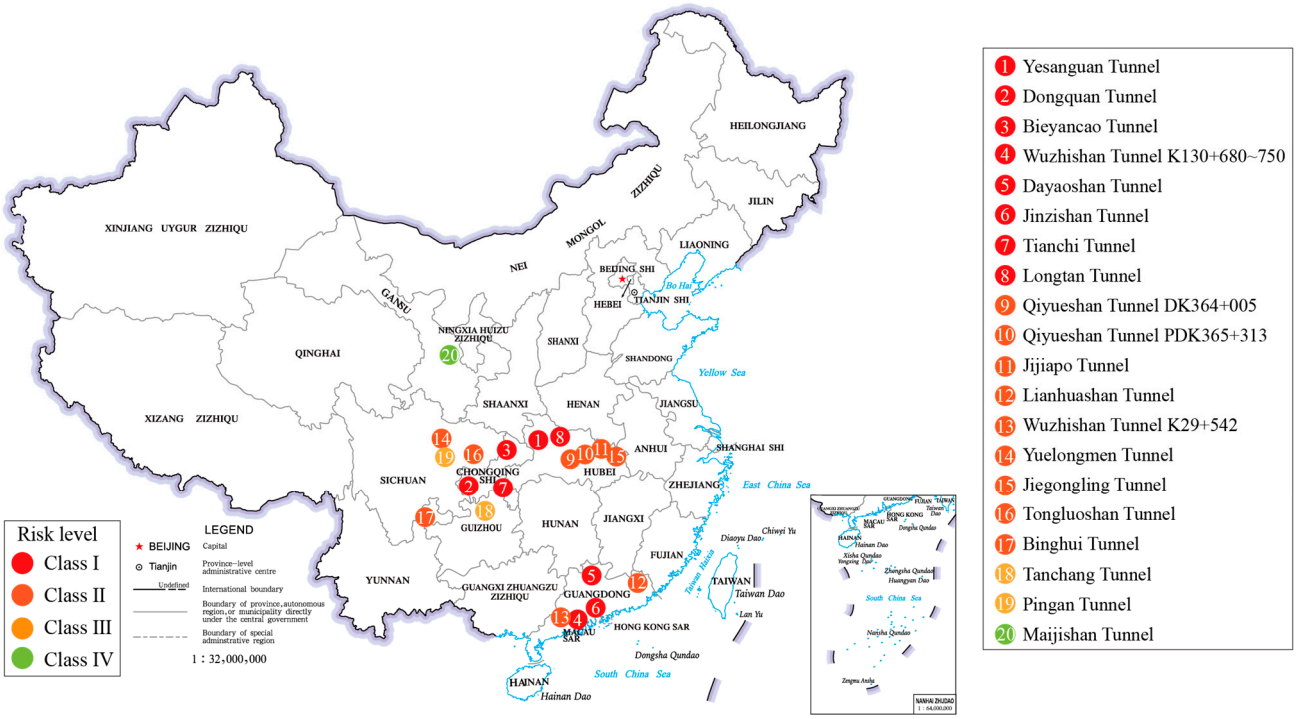

Figure 10. Geographic distribution of the 20 tunnels water inrush cases used for model validation.

The numbers correspond to the case numbers listed in Table 8. The locations are plotted according to the reported tunnel project locations. Base map source: Standard Map Service System of the Ministry of Natural Resources of China, approval number: GS (2019)1676.

Three confidence levels, namely 0.60, 0.65, and 0.70, were selected to predict the risk level and risk probability of water inrush in the 20 typical cases using the proposed model. The prediction results under the three confidence levels are shown in Figure 11, and the

overall validation results are summarised in Table 9. When the confidence level was 0.60, 16 of the 20 cases were correctly classified, corresponding to a prediction accuracy of 80%, and the misclassified cases were mainly low-risk cases. When the confidence level was 0.65, all 20 cases were correctly classified, achieving a prediction accuracy of 100%. When the confidence level was 0.70, 15 cases were correctly classified, with an accuracy of 75%, and the misclassified cases were mainly Class I and Class II cases. Therefore, the confidence level of 0.65 provided the best classification performance in the validation dataset and was adopted in the subsequent Nafeng Tunnel risk assessment.

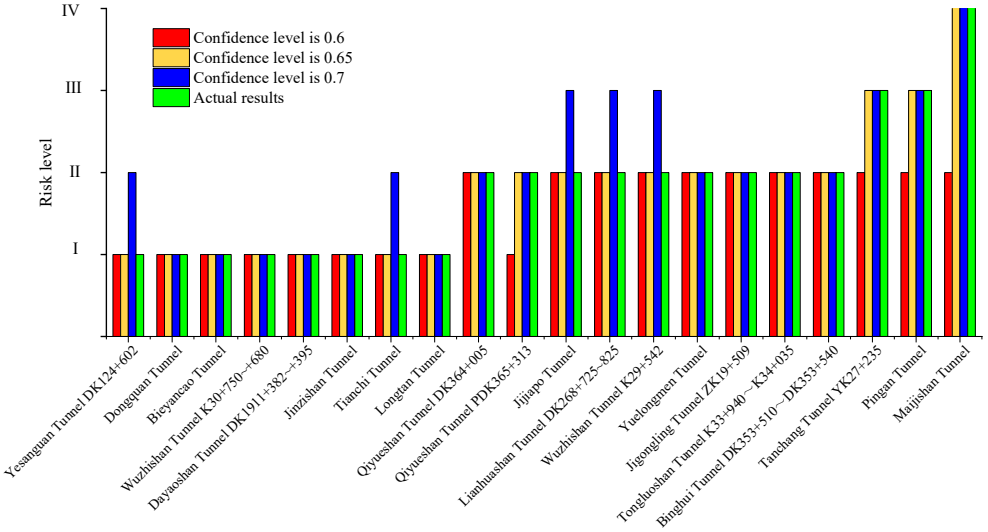

Figure 11. Comparative analysis of the prediction results.

Table 9. Validation results of the proposed model under different confidence levels.

Confidence Level	Number of Correctly Predicted Cases	Number of Incorrectly Predicted Cases	Prediction Accuracy	Main Characteristics of Misclassified Cases
0.60	16	4	80%	Mainly low-risk cases
0.65	20	0	100%	None
0.70	15	5	75%	Mainly Class I and Class II cases

4.4. Risk Assessment

Combining the geological analysis with the hybrid optimisation model, the assessment reveals that the D0 + 220.6–D0 + 285 m section of the Nafeng Tunnel falls under the Class II risk category. It presents a potential for frequent, large-scale water inrush and mud outburst incidents with a probability of 0.515. Meanwhile, the D0 + 285–D0 + 340.6 m section is subject to the same Class II risk level but with a probability of 1.0, signifying an extremely high likelihood of similar disasters.

To further support the Class II classification and clarify the influence of each parameter, the combined weights obtained using the AHP–IEM–GT method were used as relative contribution coefficients in the proposed multi-attribute decision-making framework. These coefficients indicate the relative impact of each assessment index on the comprehensive attribute measure and the final risk classification. The results are listed in Table 10. As shown in Table 10, groundwater level (I_2), formation lithology (I_1), folds distribution (I_7), and fault properties (I_8) have the highest relative sensitivity coefficients, together accounting for 66.44% of the total influence. This indicates that hydrogeological conditions, lithological characteristics, and structural geological conditions are the main controlling factors in the proposed model. For the Nafeng Tunnel, the Class II classification is mainly

associated with the groundwater conditions, fold-related structural setting, the influence of the F22-1 fault, high regional rainfall, and Class IV–V surrounding rock. It should be noted that these coefficients represent relative sensitivity within the multi-attribute decision-making framework rather than statistical regression-based sensitivity coefficients.

Table 10. Relative sensitivity coefficients of the assessment indices for the Nafeng Tunnel risk classification.

Indicator	Relative Sensitivity Coefficient	Contribution/%	Rank
Formation lithology (I_1)	0.1743	17.43	2
Groundwater level/m (I_2)	0.1801	18.01	1
Negative topography area ratio (I_3)	0.0996	9.96	5
Annual average rainfall/mm (I_4)	0.0895	8.95	6
Corrected strata angle/° (I_5)	0.0533	5.33	7
Rock quality (I_6)	0.0458	4.58	9
Folds distribution (I_7)	0.1664	16.64	3
Fault properties (I_8)	0.1436	14.36	4
Fault width/m (I_9)	0.0475	4.75	8

Synthesising the risk evaluation results for the section D0 + 220.6–D0 + 340.6 and considering the evident impact of the F22-1 fault, the following measures are suggested: intensify advanced geological forecasting and employ small-pipe advanced pre-grouting to consolidate the rock mass, block water pathways, and enlarge the scope of reinforcement. It is necessary to implement advanced support to enhance support stiffness. In scenarios characterised by large deformation of the surrounding rock or severe collapse, pipe roof support should be employed to ensure safe passage through the fault zone. In the event of severe water inflow at the tunnel face, curtain grouting or surface directional grouting should be employed for water control. It is crucial to ensure the timely closure of the support system and perform immediate backfill grouting. Furthermore, on-site monitoring of surrounding rock deformation and water seepage must be intensified.

5. Conclusions

The identification of the risk level is the basis for early warning of tunnel water inrush. Based on the AIRT, an improved risk level identification model for tunnel water inrush was established by introducing the IEM, GT, TOPSIS, and Monte Carlo technology. The water inrush risk identification process was proposed. Compared with typical cases, the present model was verified. Some meaningful conclusions are drawn as follows:

(1) The preference of the measured results of tunnel water inrush shows a certain degree of inconsistency. The present study proposed a method for calculating the index attribute measure coefficient by introducing the TOPSIS technology.
(2) In response to the insufficient prediction performance of existing models for the risk probability of tunnel water inrush, this paper proposed a risk probability evaluation method for tunnel water inrush using Monte Carlo technology.
(3) Based on 20 typical engineering cases of tunnel water inrush, the effectiveness of the present model was further verified. This provides a basis and means for evaluating tunnel water inrush and also supports the development of targeted disaster risk prevention and control measures.
(4) The risk of water inrush and mud outburst in the inlet section of the Nafeng Tunnel is classified as Class II. Primarily influenced by the F22-1 fault, this section exhibits a high probability of hazardous incidents. Therefore, it is imperative to implement integrated control measures and intensify on-site monitoring.

Author Contributions: Writing—original draft preparation, Y.H.; Formal analysis, H.S.; Resources, P.L.; Writing—review and editing, S.F. and R.C.; Visualisation, Y.H. and L.Z.; Supervision, P.L. and R.C.; Funding acquisition, R.C. All authors have read and agreed to the published version of the manuscript.

Funding: This research was funded by the Key R&D Program of Guangxi (Grant No. GuiKe FN2600640101 and GuiKe AB24010069).

Data Availability Statement: The original contributions presented in this study are included in the article. Further inquiries can be directed to the corresponding author.

Conflicts of Interest: Authors Yue Huang and Lingtao Zeng were employed by the company Guangxi Water & Power Design Institute Co., Ltd. Author Hanying Su was employed by the company Guangxi Beibu Gulf Rim Water Diversion Co., Ltd. The remaining authors declare that the research was conducted in the absence of any commercial or financial relationships that could be construed as a potential conflict of interest.

Abbreviations

The following abbreviations are used in this manuscript:

AHP	Analytic Hierarchy Process
IEM	Inverse Entropy Method
AIRT	Attribute Interval Recognition Theory
CR	Consistency Ratio
GT	Game Theory
TOPSIS	Technique for Order Preference by Similarity to Ideal Solution

References

1. Wang, Y.C.; Jing, H.W.; Yu, L.Y.; Su, H.J.; Luo, N. Set pair analysis for risk assessment of water inrush in karst tunnels. *Bull. Eng. Geol. Environ.* **2017**, *76*, 1199–1207. [CrossRef]
2. Li, S.C.; Xu, Z.H.; Huang, X.; Lin, P.; Zhao, X.C.; Zhang, Q.S.; Yang, L.; Zhang, X.; Sun, H.F.; Pan, D. Classification, geological identification, hazard mode, and typical case studies of hazard-causing structures for water and mud inrush in tunnels. *Chin. J. Rock Mech. Eng.* **2018**, *37*, 1041–1069. [CrossRef]
3. Liang, Y.; Sui, W.; Qi, J. Experimental investigation of chemical grouting of inclined fracture to control sand and water flow. *Tunn. Undergr. Space Technol.* **2019**, *83*, 82–90. [CrossRef]
4. Li, L.P.; Jin, H.; Tu, W.F.; Zhou, Z.Q. Study on the minimum safe thickness of water inrush prevention in karst tunnel under the coupling effect of blasting power and water pressure. *Tunn. Undergr. Space Technol.* **2024**, *153*, 105994. [CrossRef]
5. Li, S.C.; Liu, C.; Zhou, Z.Q.; Li, L.P.; Shi, S.S.; Yuan, Y.C. Multisources information fusion analysis of water inrush disaster in tunnels based on improved theory of evidence. *Tunn. Undergr. Space Technol.* **2021**, *113*, 103948. [CrossRef]
6. Xue, Y.G.; Kong, F.M.; Qiu, D.H.; Su, M.X.; Zhao, Y.; Zhang, K. The classifications of water and mud/rock inrush hazard: A review and update. *Bull. Eng. Geol. Environ.* **2021**, *80*, 1907–1925. [CrossRef]
7. Zarei, H.R.; Uromeihy, A.; Sharifzadeh, M. Evaluation of high local groundwater inflow to a rock tunnel by characterization of geological features. *Tunn. Undergr. Space Technol.* **2011**, *26*, 364–373. [CrossRef]
8. Borg, A.; Bjelland, H.; Nja, O. Reflections on Bayesian Network models for road tunnel safety design: A case study from Norway. *Tunn. Undergr. Space Technol.* **2014**, *43*, 300–314. [CrossRef]
9. Niu, F.Y.; Cai, Y.C.; Liao, H.J.; Li, J.G.; Tang, K.J.; Wang, Q.; Wang, Z.C.; Liu, D.D.; Liu, T.; Liu, C.; et al. Unfavorable geology and mitigation measures for water inrush hazard during subsea tunnel construction: A global review. *Water* **2022**, *14*, 1592. [CrossRef]
10. Li, L.P.; Tu, W.F.; Yuan, Y.C.; Cheng, S.; Shi, S.S. Real-time monitoring and early warning method of disaster precursor induced by serious water inrush in underground engineering. *Oxid. Commun.* **2016**, *39*, 1108–1118.
11. Bai, J.W.; Li, S.C.; Liu, R.T.; Zhang, Q.S.; Zhang, H.J.; Sha, F. Multi-field information monitoring and warning of delayed water bursting in deep rock fault. *Chin. J. Rock Mech. Eng.* **2015**, *34*, 2327–2335. [CrossRef]
12. Li, S.C.; Wang, K.; Li, L.P.; Zhang, Q.S.; Hu, C.; Zhou, Y.; Liu, H.L.; Lin, P. Development and application of an extendable model test system for water inrush simulation in subsea tunnel. *Chin. J. Rock Mech. Eng.* **2014**, *33*, 2409–2418. [CrossRef]
13. Li, S.C.; Liu, H.L.; Li, L.P.; Zhang, Q.Q.; Wang, K.; Wang, K. Large scale three-dimensional seepage analysis model test and numerical simulation research on undersea tunnel. *Appl. Ocean Res.* **2016**, *59*, 510–520. [CrossRef]

14. Li, L.P.; Sun, S.Q.; Wang, J.; Song, S.G.; Fang, Z.D.; Zhang, M.G. Development of compound EPB shield model test system for studying the water inrushes in karst regions. *Tunn. Undergr. Space Technol.* **2020**, *101*, 103404. [CrossRef]
15. Meguid, M.A.; Saada, O.; Nunes, M.A.; Mattar, J. Physical modeling of tunnels in soft ground: A review. *Tunn. Undergr. Space Technol.* **2008**, *23*, 185–198. [CrossRef]
16. Jiang, H.M.; Li, L.; Rong, X.L.; Zhang, Z.C. Model test to investigate waterproof-resistant slab minimum safety thickness for water inrush geohazards. *Tunn. Undergr. Space Technol.* **2017**, *62*, 35–42. [CrossRef]
17. Ma, D.; Rezania, M.; Yu, H.S.; Bai, H.B. Variations of hydraulic properties of granular sandstones during water inrush: Effect of small particle migration. *Eng. Geol.* **2017**, *217*, 61–70. [CrossRef]
18. Yang, W.; Fang, Z.; Yang, X.; Shi, S.; Wang, J.; Wang, H.; Bu, L.; Li, L.; Zhou, Z.; Li, X. Experimental study of influence of karst aquifer on the law of water inrush in tunnels. *Water* **2018**, *10*, 1211. [CrossRef]
19. Zhao, Y.; Yang, T.H.; Deng, W.X.; Zhou, G.L.; Wang, S.H.; Zhao, Q.B.; Cao, Y.S. Location and mechanism analysis of curtain water inrush channels based on MTI-derived parameters—A case study. *Tunn. Undergr. Space Technol.* **2023**, *141*, 105357. [CrossRef]
20. Wang, J.; Zhang, Y.; Qin, Z.; Song, S.G.; Lin, P. Analysis method of water inrush for tunnels with damaged water-resisting rock mass based on finite element method-smooth particle hydrodynamics coupling. *Comput. Geotech.* **2020**, *126*, 103725. [CrossRef]
21. Fan, H.Y.; Li, L.P.; Chen, G.Q.; Liu, H.L.; Gao, J.Y.; Li, C.; Peng, X.; Zhou, S. Analysis method of the water inrush and collapse in jointed rock mass tunnels: A case study. *Eng. Anal. Bound. Elem.* **2023**, *146*, 838–850. [CrossRef]
22. Gao, J.Y.; Peng, S.Y.; Chen, G.Q.; Mitani, Y.; Fan, H.Y. Coupled hydro-mechanical analysis for water inrush of fractured rock masses using the discontinuous deformation analysis. *Comput. Geotech.* **2023**, *156*, 105247. [CrossRef]
23. Liu, J.Q.; Sun, Y.K.; Li, C.J.; Yuan, H.L.; Chen, W.Z.; Liu, X.Y.; Zhou, X.S. Field monitoring and numerical analysis of tunnel water inrush and the environmental changes. *Tunn. Undergr. Space Technol.* **2022**, *122*, 104360. [CrossRef]
24. Ma, K.; Sun, X.Y.; Tang, C.A.; Yuan, F.Z.; Wang, S.J.; Chen, T. Floor water inrush analysis based on mechanical failure characters and microseismic monitoring. *Tunn. Undergr. Space Technol.* **2021**, *108*, 103698. [CrossRef]
25. Huang, Z.; Zhao, K.; Li, X.Z.; Zhong, W.; Wu, Y. Numerical characterization of groundwater flow and fracture-induced water inrush in tunnels. *Tunn. Undergr. Space Technol.* **2021**, *116*, 104119. [CrossRef]
26. Mahmoodzadeh, A.; Mohammadi, M.; Noori, K.M.G.; Khishe, M.; Ibrahim, H.H.; Hama Ali, H.F.; Abdulhamid, S.N. Presenting the best prediction model of water inflow into drill and blast tunnels among several machine learning techniques. *Autom. Constr.* **2021**, *127*, 103719. [CrossRef]
27. Peng, F.L.; Dong, Y.H.; Wang, W.X.; Ma, C.X. The next frontier: Data-driven urban underground space planning orienting multiple development concepts. *Smart Constr. Sustain. Cities* **2023**, *1*, 3. [CrossRef]
28. Zhang, N.; Niu, M.; Wan, F.; Lu, J.; Wang, Y.; Yan, X.; Zhou, C. Hazard prediction of water inrush in water-rich tunnels based on random forest algorithm. *Appl. Sci.* **2024**, *14*, 867. [CrossRef]
29. Aalianvari, A.; Katibeh, H.; Sharifzadeh, M. Application of fuzzy Delphi AHP method for the estimation and classification of Ghomrud tunnel from groundwater flow hazard. *Arab. J. Geosci.* **2012**, *5*, 275–284. [CrossRef]
30. Wang, Y.C.; Yin, X.; Jing, H.W.; Liu, R.C.; Su, H.J. A novel cloud model for risk analysis of water inrush in karst tunnels. *Environ. Earth Sci.* **2016**, *75*, 1450. [CrossRef]
31. Luo, M.M.; Chen, J.; Jakada, H.; Li, N.; Guo, X.L.; Zhou, H. Identifying and predicting karst water inrush in a deep tunnel, South China. *Eng. Geol.* **2022**, *305*, 106716. [CrossRef]
32. Jolfaei, S.; Lakirouhani, A. Sensitivity analysis of effective parameters in borehole failure, using neural network. *Adv. Civ. Eng.* **2022**, *2022*, 4958004. [CrossRef]
33. Wang, S.; Li, L.P.; Cheng, S.; Yang, J.Y.; Jin, H.; Gao, S.; Wen, T. Study on an improved real-time monitoring and fusion prewarning method for water inrush in tunnels. *Tunn. Undergr. Space Technol.* **2021**, *112*, 103884. [CrossRef]
34. Zhang, W.; Zhou, X.; Wei, W.; Cheng, X. Risk assessment of water inrush in tunnels: A case study of a tunnel in Guangdong Province, China. *Sustainability* **2022**, *14*, 11443. [CrossRef]
35. Kong, H.Q.; Zhang, N. Risk assessment of water inrush accident during tunnel construction based on FAHP-I-TOPSIS. *J. Clean. Prod.* **2024**, *449*, 141744. [CrossRef]
36. Wang, S.; Li, L.P.; Cheng, S.; Hu, H.J.; Zhang, M.G.; Wen, T. Risk assessment of water inrush in tunnels based on attribute interval recognition theory. *J. Cent. South Univ.* **2020**, *27*, 517–530. [CrossRef]
37. Wu, B.; Chen, H.H.; Meng, G.W.; Huang, W.; Cai, J.; Li, Y.; Zhang, Y. A dynamic assessment method on collapse risk of small spacing tunnels based on attribute interval recognition model. *Arab. J. Geosci.* **2021**, *14*, 2545. [CrossRef]
38. Wu, B.; Chen, H.H.; Huang, W.; Meng, G.W. Dynamic evaluation method of the EW-AHP attribute identification model for the tunnel gushing water disaster under interval conditions and applications. *Math. Probl. Eng.* **2021**, *2021*, 6661609. [CrossRef]
39. Wang, B.; Li, Q.K.; Xu, Z.F.; Niu, S.B.; Nie, X.T. A safety risk assessment method for TBM tunnel construction based on attribute interval identification theory. *Sci. Rep.* **2025**, *15*, 7673. [CrossRef]
40. Zhou, Z.Q.; Kong, J.; Yang, W.M.; Chen, Y.P.; Zhang, Q.; Li, L.P.; Shi, S.S. Improved attribute interval recognition method and its application in risk assessment of water inrush in tunnels. *J. Cent. South Univ. Sci. Technol.* **2020**, *51*, 1703–1711. [CrossRef]

41. Yin, X.; Liu, Q.S.; Wang, X.Y.; Huang, X. Prediction model of rockburst intensity classification based on combined weighting and attribute interval recognition theory. *J. China Coal Soc.* **2020**, *45*, 3772–3780. [CrossRef]
42. Lyu, H.M.; Sun, W.J.; Shen, S.L.; Zhou, A. A risk assessment using a new consulting process in fuzzy AHP. *J. Constr. Eng. Manag.* **2020**, *146*, 04019112. [CrossRef]
43. Wang, W.; Li, H.; Hou, X.; Zhang, Q.; Tian, S. Multi-criteria evaluation of distributed energy system based on order relation-anti-entropy weight method. *Energies* **2021**, *14*, 246. [CrossRef]
44. Esposito, C.; Ficco, M.; Palmieri, F.; Castiglione, A. Smart cloud storage service selection based on fuzzy logic, theory of evidence and game theory. *IEEE Trans. Comput.* **2015**, *64*, 2348–2362. [CrossRef]
45. Xu, Z.H.; Li, S.C.; Li, L.P.; Chen, J.; Shi, S.S. Construction permit mechanism of karst tunnels based on dynamic assessment and management of risk. *Chin. J. Geotech. Eng.* **2011**, *33*, 1714–1725.
46. Li, S.C.; Zhou, Z.Q.; Li, L.P.; Shi, S.S.; Xu, Z.H. Risk evaluation theory and method of water inrush in karst tunnels and its applications. *Chin. J. Rock Mech. Eng.* **2013**, *32*, 1858–1867. [CrossRef]
47. Wu, Z.J.; Dai, Q.; Chu, Z.F.; Liu, Q.S.; Chen, J.; You, W.J. Risk prediction of water inrush in karst tunnels based on DNN and attribute mathematics. *China J. Highw. Transp.* **2024**, *37*, 82–99. [CrossRef]
48. *GB/T 50218-2014 [S]*; Standard for Engineering Classification of Rock Mass. China Planning Press: Beijing, China, 2015.
49. Li, S.C.; Xue, Y.G.; Zhang, Q.S.; Li, S.C.; Li, L.P.; Sun, K.G.; Ge, Y.H.; Su, M.X.; Zhong, S.H.; Li, X. Key technology study on comprehensive prediction and early warning of geological hazards during tunnel construction in high-risk karst areas. *Chin. J. Rock Mech. Eng.* **2008**, *27*, 1297–1307. [CrossRef]

Disclaimer/Publisher's Note: The statements, opinions and data contained in all publications are solely those of the individual author(s) and contributor(s) and not of MDPI and/or the editor(s). MDPI and/or the editor(s) disclaim responsibility for any injury to people or property resulting from any ideas, methods, instructions or products referred to in the content.